Manuscript

SLM-processed Sc- and Zr- modified Al-Mg alloy: Mechanical properties and microstructural effects of heat treatment

A.B. Spierings[1], K. Dawson[2], K. Kern[3], F. Palm[4], K. Wegener[5]

[1] Innovation Centre for Additive Manufacturing, INSPIRE-AG, Lerchenfeldstrasse 5, CH-9014 St.Gallen, Switzerland
[2] Centre for Materials and Structures, School of Engineering, University of Liverpool, Liverpool L69 3GH, UK
[3] University of Applied Sciences NTB, CH- Buchs, Switzerland
[4] Airbus Group Innovations TX1M, D-81663 Munich, Germany
[5]Institute of Machine Tools and Manufacturing,, Department of Mechanical and Process Engineering, ETH Zurich, CH-8092 Zurich, Switzerland

Abstract

Traditionally 4xxx casting alloys are used for the additive manufacturing of structurally optimised lightweight parts in space, aerospace and automotive. However, for such applications there is a need for hardenable high-strength Al-alloys exceeding the properties of the 4xxx alloys family. The study analyses the hardness response of different heat treatment temperatures and hold durations applied to a Sc- and Zr-modified Al-Mg (5xxx-) alloy (Scalmalloy®) processed by Selective Laser Melting, and compares the mechanical properties and microstructure in the as-processed and annealed condition. The results show that the static mechanical properties are exceptionally good with R_m-values exceeding 500MPa along with almost no build-orientation related anisotropic effects, and a high ductility even in the heat treated condition, and these properties are clearly related to the very fine grained material. The stress-strain curves show the typical Portevin-Le-Chatelier (PLC) effect as known for other 5xxx alloys. Due to significant grain boundary pinning by different particles the very fine-grained bi-modal microstructure originating from the SLM-process can be maintained even in the heat treated condition, and only a HIP treatment leads to local grain growth only in coarser grained regions.

Keywords: Powder methods, Selective Laser Melting, Aluminium alloys, Characterization, stress-strain measurements, hardness

1 Introduction

In many industrial sectors like space, aerospace and automotive, the performance of (metal) products depends on their weight. Weight reduction can be achieved by structural optimization, and the use of lightweight alloys like aluminium or titanium. Thereby, the weight reduction potential depends on the ability to produce parts with high structural complexity, as it is achieved e.g. by topology optimization, and the specific mechanical strength of the alloys used.

Additive manufacturing (AM) is able to fulfill both requirements. The technological benefits of AM come into effect especially at the production of parts with a complexity exceeding the possibilities of conventional manufacturing technologies. On the other hand, lightweight alloys like titanium and aluminium are readily processed by metal additive manufacturing such as Selective Laser Melting (SLM) once the process window for the specific alloy has been found.

State-of-the-art in SLM of aluminium are mainly 4xxx alloys, e.g. AlSi12[1-3], AlSi10Mg [4-7] or AlSi7Mg0.3 [8]. Their near-eutectic compostion facilitates SLM-processing due to the short solidification range, and the associated lowered risk of cracking. Good mechanical performances are reported for such alloys especially in the heat treated condition [3, 4, 9], although microstructure-related anisotropic effects with regard to the additive build orientation are evident, as reported by e.g. by Tang [10], and need to be considered. However, for structural applications in above mentioned sectors, hardenable 2xxx, 6xxx or 7xxx alloys are preferred. The SLM-processing of such alloys on the other hand is more difficult due to their potential for hot cracking once the process window for the specific alloy has been found. Therefore

alloy modifications can be a possible route to overcome potential processing constraints, leading to 'alloys for AM (SLM)'. That such an approach can be successful has been proven by Montero Sistiaga [11], who added Si to an Al-7075 alloy to at least minimize its hot cracking potential during SLM.
A newer SLM-processable and heat treatable Sc- and Zr-modified 5xxx alloy with significant advantages is the Scalmalloy® alloy system. In [12] the microstructure and related formation mechanisms of Scalmalloy® during SLM-processing have been presented in detail. This alloy offers high strength and ductility already in the as-processed condition, combined with comparably low anisotropic mechanical behaviour e.g. in $R_{P0.2}$, as discussed by Schmidke [13] and Spierings [14]. By this the mechanical properties exceed reported values for traditional alloys like AlSi10Mg or AlSi12 [1-3, 5, 15]. Schmidke [13] discussed the static mechanical performance of heat treated samples in the 0°-, 45°- and 90° orientation, and found a very ductile fracture behaviour along the maximum shear stress orientation (fracture plane in 45° to the load direction). The tensile strength exceeded 520MPa for all directions, having only a low anisotropy, which is consistent with initial findings discussed in [14]. The low anisotropy is related to the comparably fine grained microstructure with a high amount of equiaxed grains, and ageing improves the mechanical performance in Sc- and Zr-containing alloys due to the precipitation of (additional) $Al_3(Sc_x\ Zr_{1-x})$ particles from solid solution, as has been discussed for instance by Røyset [16] for a cast Al-0.2wt%Sc alloy, or by Fuller et al. [17] for various Al-alloys with Sc weight-contents between 0.1% and 0.3%, and Zr weight-contents between 0% and 0.16%, respectively.
Literature reports about a wide range of ageing temperatures and times used for such alloys. Davydov et al. [18] analysed the microhardness evolution for temperatures between 300°C and 500°C for an AlSc0.4, and for an AlSc0.2 alloy at 400°C and 450°C, each with and without an addition of 0.15wt% Zr. He found a very rapid hardening response of <1h for temperatures ≥≈ 350°C, and much slower behaviour at 300°C. Zr is reported to stabilize the microstructure, and to increase the strengthening remarkably. These findings are in good agreement with the ones from Fuller et al. [17], who used temperatures of 300°C, 350°C and 375°C and ageing times up to ≈100h. Røyset [16] investigated the fraction of transformed Al_3Sc at temperatures between 230°C and 470°C for hold durations up to ≈20h, and constructed a time-temperature-transformation (TTT) diagram. He found a transformation time minimum at ≈310°C (≈ 4h for 95% transformation) for the coherent precipitation, and a time minimum at ≈410°C where discontinuous precipitation dominates.

This paper discusses the development of a post-process heat treatment for a SLM-processed Sc- and Zr-modified 5xxx Al-alloy (Scalmalloy®), and presents the effects of a post-process heat treatment and HIP-processing on the static mechanical properties. The results are complemented with a microstructural comparison to the as-processed condition. Presented data provide an engineering starting point to design additively manufacture structural parts from that alloy.

2 Methods and Materials

2.1 Sample production with SLM

The Scalmalloy® powder material with nominal composition of Al4.6Mg0.66Sc0.42Zr0.49Mn was used in a ConceptLaser M2 machine equipped with a 200W Gaussian Nd-YAG laser operated in cw mode. All samples were produced in a N_2 atmosphere using the maximum laser power available, and a 30µm slice thickness. Details on the processing window development are presented by Spierings [14]. 10x10x10mm^3 cube samples were produced for the analysis of material hardness and microstructure, whereas static tensile test specimens were produced as cylinders with a length of 80mm and a diameter of 7mm in horizontal (90°) and vertical (0°) build orientation to analyse mechanical properties using scan speeds of 170mms^{-1} and 300mms^{-1}.
For the heat treatment development, samples were produced at scan speeds of 170 mms^{-1} or 250 mms^{-1}. The energy density E_V used to produce the samples is calculated according to equation 1, with P the laser power, v_s the laser spot scan speed, d the hatch distance and t the slice thickness.

$$E_V = \frac{P}{v_s \cdot d \cdot t} \quad (1)$$

The tensile test samples were produced and analysed in different configurations: The E_V-levels were 135 Jmm^{-3} and 238 Jmm^{-3} corresponding to a scan speed of 300 mms^{-1} and 170 mms^{-1}, respectively, and surfaces were either in the as-built and peened condition, or the raw samples were machined to the final specimen geometry according to DIN-50'125-A5 with a surface roughness of N6 (R_a = 0.8 µm) or better, except for the HIPed samples which were turned according to DIN-50'125-B5x25. Samples were tested in the as-built and in different heat treated conditions, including hot isostatic pressure (HIP). For each configuration (build orientation, processing window, heat treatment) at least five specimens were prepared. Details on the sample configuration are indicated in the corresponding results section.

Additionally to the static testing of cylindrical tensile samples, flat dog-bone like specimens according to Figure 1 with a thickness of 2.0 ± 0.02 mm were manufactured in a horizontal and vertical build orientation and HIPed (see below). These samples were used for optical space-resolved 2-dimensional strain monitoring by Digital Image Correlation, and the real Poisson constant of the alloy. The final samples were coated / sprayed with black-and-white dots in order to get optically traceable reference points.

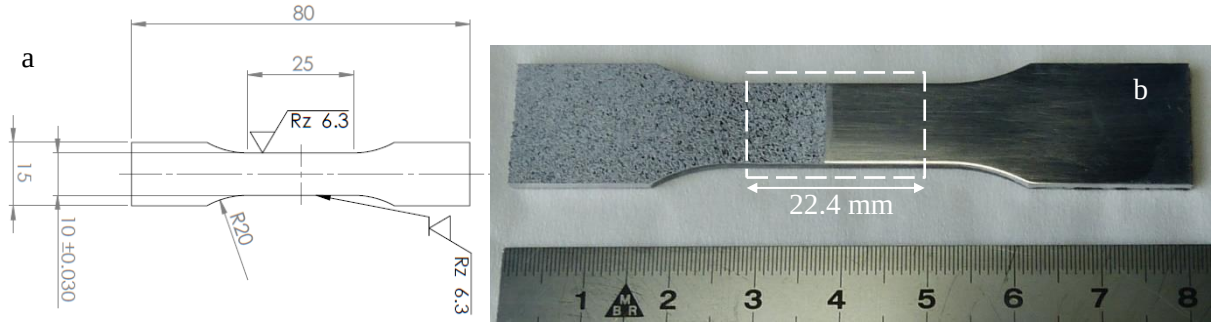

Figure 1: a) Geometry of dog-bone like tensile test specimens. b) Image montage of the final prepared sample with left side coated surface, and right side as-peened surface. Dashed frame corresponds approximately to the measurement area with a length of 22.4 mm (Figure 7)

2.2 Post-process heat treatment and HIP procedure

In order to promote controlled precipitation of $Al_3(Sc_1\ Zr_{1-x})$ particles a post-process ageing procedure was optimized for temperature and hold duration in two steps, using a ThermConcept KM/3 heat treatment oven and N_2 atmosphere.

In order to determine relevant heat temperature ranges where precipitation occurs, heat treatments at temperatures between 250°C and 500°C (at steps of 50K) are applied for 4h on samples processed at v_s = 170 mms^{-1}. This temperature range follows approximately the range used by Røyset [16] in the analysis of the Sc-fraction transformed to Al_3Sc particles, when he calculated the n-values for the Johnson-Mehl-Avrami-Kolmogorov (JMAK) relationship of transformation. This range also covers the aging times and temperatures used by Fuller [17] for different Al-Sc-Zr alloys. In addition the effects of hold duration was analysed on samples processed at v_S = 250 mms^{-1}. Hold durations of 0.5h, 1h, 2h, 5h, 10h and 24h were used for temperatures of 275°C, 325°C and 375°C.

A HIP-process was performed at operating conditions over 1'000bar, 325°C / 4h. This annealing temperature and time is based on the results from previous annealing tests. The data serve for comparison of pore-free material with SLM-processed, defect containing material.

2.4 Hardness measurement

The characterization of the effect of a post-process annealing procedure on material hardness was performed using a Gnehm Brickers 220 hardness tester; results are reported in Brinell hardness (HB) values. Alternatively a hardness tester LVD-302 was also used (measuring Vickers hardness and being

converted into HB for better comparison). Three to five measurements from each of the differently processed samples were taken and mean value and standard deviation are calculated.

2.5 Mechanical characterization

Static mechanical testing was performed on a Walter&Bai hydraulic tensile testing machine LFV-25, equipped with a clip-on axial extensometer type MFA 25 (L_0 = 25mm) for strain measurement. Testing was performed in accordance with DIN EN ISO 6892-1. From the measured "engineering" stress-strain curves gained from quasi-static tensile testing, the true (index 'T') stress-strain curves and true ultimate strength ($R_{m,T}$) is calculated for the plastic region according to Hosford [19] by

$$\sigma_T = \sigma \cdot (1 + \varepsilon); \quad R_{m,T} = R_m \cdot (1 + \varepsilon); \quad \epsilon_T = ln(1 + \varepsilon) \tag{3}$$

The dog-bone samples were tested in a Zwick/Roell Z100 AllroundLine testing machine. Space-resolved strain monitoring was performed with 2 optical cameras using the Dantec Digital Image Correlation system, and the ISTRA 4D software (V4.4.4 Q-400 3D).

2.6 Microstructural analysis

The samples' microstructure were analysed by a FEI Helios dual beam FIB instrument equipped with an EDAX-EBSD / EDS Tenupol-3 twin jet electro-polisher and a 5vol-% perchloric acid in 95vol-% methanol electrolyte, cooled to -50°C with a voltage of 25V. The cutting plane orientation was in the yz-plane, hence parallel to the z the build direction and in x- or y-scan direction (Figure 2).

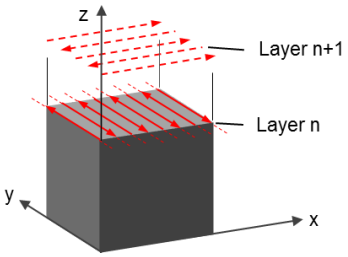

Figure 2: SLM sample build strategy and coordinate system

TEM analysis was performed in a probe side aberration corrected JEOL 2100FCS microscope operated at 200kV. Both bright field (BF) and high angle annular dark field (HAADF) images were captured in scanning transmission electron microscopy (STEM) mode. Scattered electrons were collected using a HAADF detector over a semi-angle ranging from 70 - 190mrad to produce z-sensitive dark field images.

3 Results

3.1 Material hardness

The hardness evolution of samples processed at 170mms^{-1} and heat treated at temperatures between 250°C and 500°C for 4h is shown in Figure 3. Up to 400°C hardness increases due to the formation of fine nm-scaled Al_3(Sc, Zr) precipitates, as also observed by other research on the Sc-effect in conventional Al-alloys (e.g. Røyset [16], Fuller [17], Milman [20]).

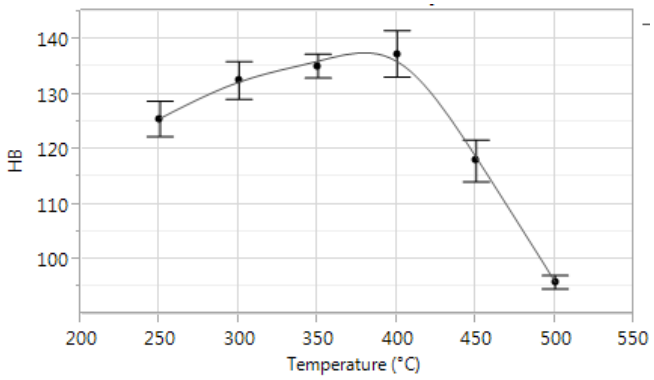

Figure 3: Hardness evolution from annealing for 4h at temperatures between 250°C and 500°C. Error bars indicate standard deviation (n=5)

At higher temperatures exceeding 400°C (at hold duration of 4h), hardness reduces significantly to values below the as-processed hardness of 101HB (processed at 170 mms^{-1}). Based on these hardness results it becomes clear that any ageing should take place at temperatures clearly below 400°C to prevent Ostwald ripening by too large $Al_3(Sc,Zr)$ precipitates, which lose their coherency when it becomes more favourable to introduce a dislocation at the particle interface than increasing even more the matrix strain around that particle. Coherency loss is reported to take place at sizes of ≈ 21.5 nm [21].
Figure 4 shows the hardness evolution for annealing temperatures of 275°C, 325°C and 375°C for hold durations between 0.5h and 24h. It appears that 275°C is not sufficient to reach full hardness, as even after prolonged ageing times hardness still increases. At 375°C the hardness increase takes place much more rapidly and already after 0.5h full hardness is achieved, whereas at ageing times > 10h indications of overageing are observable.

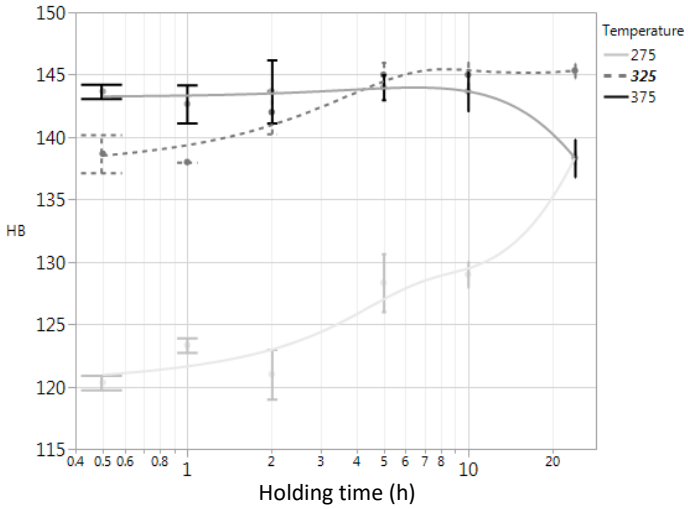

Figure 4: Hardness evolution at 275°C, 325°C and 375°C at different hold durations (log-scale). Error bars = one standard deviation (n=3)

For an ageing temperature of 325°C full hardness is achieved after ≈5h, without signs of overageing at longer hold durations, which makes this temperature level to be considered as very reliable.

3.2 As-processed static mechanical properties

No statistically significant (α=0.05) differences were found for vertically built samples (E_V = 238Jmm^{-3}) with turned or as-built and peened surface, having a pooled mean true strength of 427 ± 8 MPa, and $R_{P0.2}$ = 287 ± 3 MPa. However, this is not true for E-Modulus, which is 68.7 ± 1.2 GPa for turned surfaces, and 58.5 ± 1.8 GPa for as-processed and peened surface. For this reason no difference is taken with regard to the surface condition in the following strengths analysis.
The comparison of vertically and horizontally built samples at 170 mms^{-1} and 300 mms^{-1} is presented in Figure 5, showing a very small anisotropy in tensile strength. The true ultimate tensile strengths in 0° and 90° direction show differences of 2.6% and 2.7%, respectively. For yield strength the variation is somewhat higher with 3.8% and 10.8%.

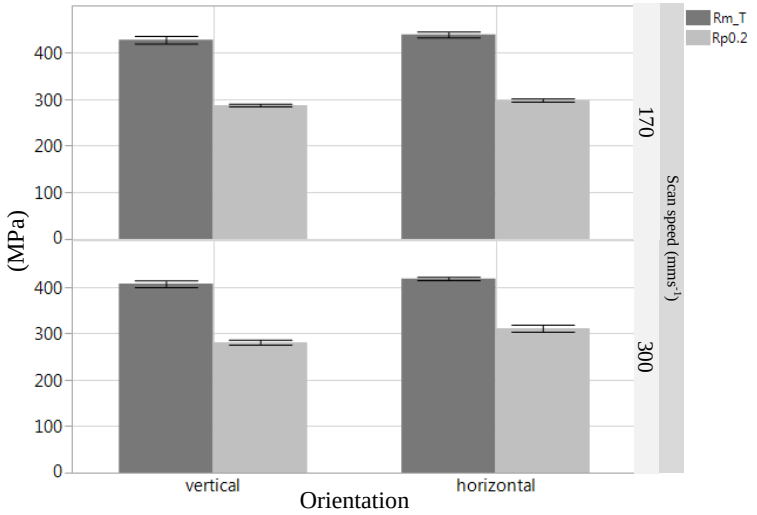

Figure 5: Box-plot for as-built true stress R_{m_T} and $R_{p0.2}$ at 170 mms^{-1} and 300mms^{-1} for horizontal and vertical build orientation.

The differences in $R_{m,T}$ and $R_{p0.2}$ between the two v_s-levels in the as-processed condition (Figure 5) are comparably small. However, it must be expected that scan speed-related differences on the microstructural level exist, which are responsible for the small but significant differences. These aspects are not discussed here.

A number of near-surface pores were observed around at the periphery of fracture surfaces. Although on occasion, these pores were seen to have 'opened', they did not appear to have been instrumental in the fracture process and fracture commenced in a ductile manner.

Table 2 shows the fracture surfaces of as-built horizontal and vertical tensile test samples. Most of the samples fractured under an angle of ≈45° to the load axis, hence in the direction of maximum shear stresses. Furthermore, the fracture surfaces show ductile fracture behaviour, with some typical dimples. Correspondingly the elongation to fracture is quite large, as shown in Table 1.

Table 1: Elongation to fracture ($A_{5.65}$) in the as-built condition for the two v_s regimes

scan speed v_s	0° / vertical	90° / horizontal
170 mms^{-1}	17.2% ± 1.6%;	20.2% ± 1.9%;
300 mms^{-1}	14.2% ± 1.5%;	17.8% ± 1.9%.

A number of near-surface pores were observed around at the periphery of fracture surfaces. Although on occasion, these pores were seen to have 'opened', they did not appear to have been instrumental in the fracture process and fracture commenced in a ductile manner.

Table 2: Fracture surfaces of as-built vertical and horizontal samples

vertical build orientation	horizontal build orientation
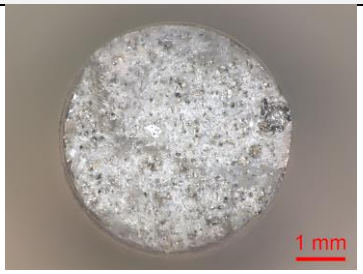	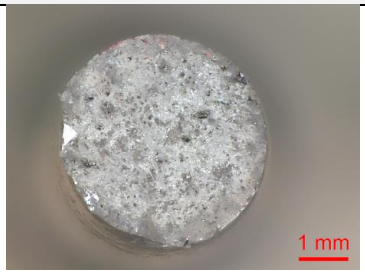

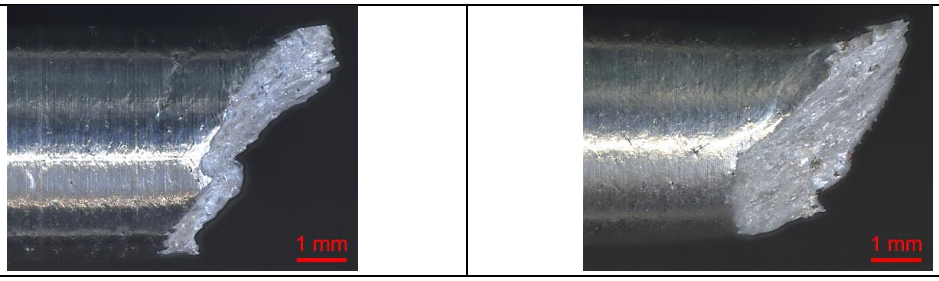

3.3 Heat treated static mechanical properties

Figure 6 shows true and yield strength for vertically built (0°) samples, heat treated between 300°C and 400°C, and for annealing times of 4h, 6h and 8h. Note: Not all combinations of heat treatment temperatures and holding durations were analysed here, but these data complement the results from Figure 4 showing that annealing at 300°C/4h does not yet yield to the maximum strength, although differences to 350°C are comparably small. Ageing at higher temperatures and hold durations lead to over-ageing and consequently to lower mechanical strength.

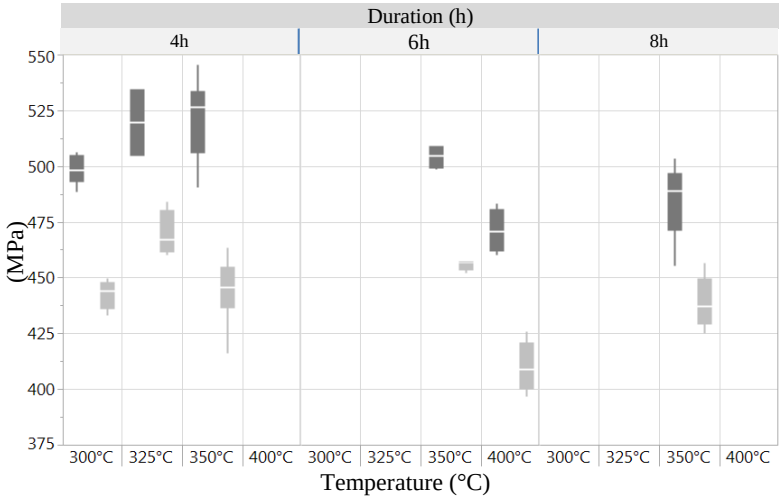

Figure 6: True stress (■ R_{m_T}) and yield strength (■ $R_{P0.2}$) for vertically built specimens (170mms^{-1}) at 300°C to 400°C and hold durations between 4h and 8h.

The results shown in Figure 6 point out that a heat treatment between 325°C / 4h and 350°C / 4h seems to be optimal, reaching $R_{m,T}$ = 515 ± 16 MPa, $R_{P0.2}$ = 450 ± 9 MPa and E = 72.3 ± 3.8 GPa for the vertical build orientation (N = 14). For the horizontal build orientation, the corresponding results are $R_{m,T}$ = 530 ± 12 MPa, $R_{P0.2}$ = 453 ± 20 MPa and E = 71.8 ± 2.5 GPa (N = 13), respectively. Hence, the differences in $R_{m,T}$ are statistically significant, although comparably small, whereas differences in E and $R_{P0.2}$ were not significant (p = 0.05).

The optical strain monitoring on the dog-bone samples is shown in the image sequence in Figure 7. It shows at the beginning very local strain- (stress-) concentrations (Figure 7a), most probably on small surface-near defects such as pores etc. As soon as the yield strength is exceeded, well defined strain fields (possibly Lüders Bands) develop (Figure 7b) and propagate for increasing strain (Figure 7c). The high yield followed by a drop in stress required for continued flow of the heat treated / HIPed samples shown in Figure 8 might be consistent with such Lüders Bands. Right before the fracture occurs at a local maximum strain of ≈ 24% the sample begins to significantly been narrowed (Figure 7d), whereas at the point of fracture the local strain reaches values exceeding 30% (Figure 7e). The evaluated E-modulus in the HIP-condition is 74.5GPa, which is in good agreement with the data acquired from stress-strain measurements using the strain gauge. From the data in the elastic region the Poisson constant was evaluated, which is as expected ν = 0.33 for both build orientations.

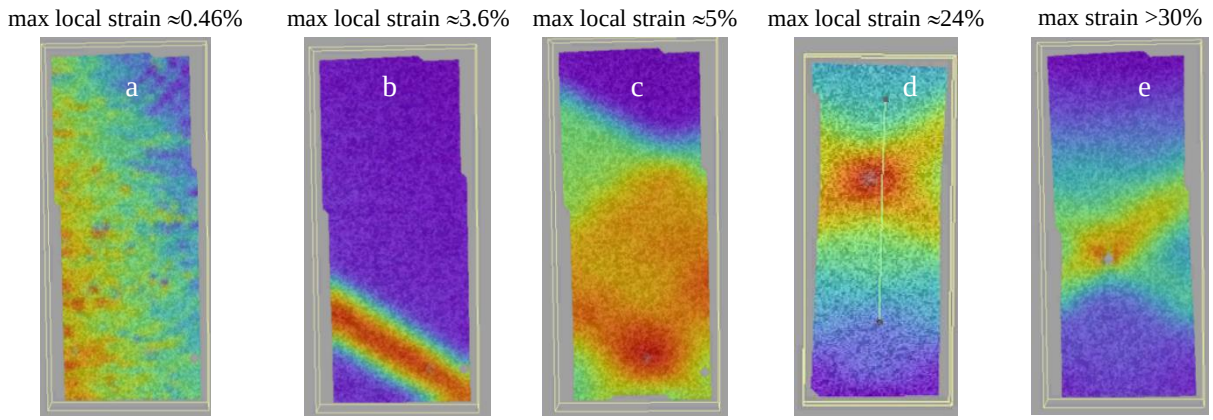

Figure 7: Optical strain monitoring on a middle measurement section of dog-bone samples with a length of 22.4 mm. Engineering strain in z-direction (dynamically adjusted strain colour)

Figure 8 shows the measured true stress-strain curves (using the strain gauge) for horizontal and vertical build orientations, and for the as-processed, heat treated and HIPed conditions. Obviously there is almost no anisotropy in the stress-strain behaviour with regard to the build orientation between the three conditions.

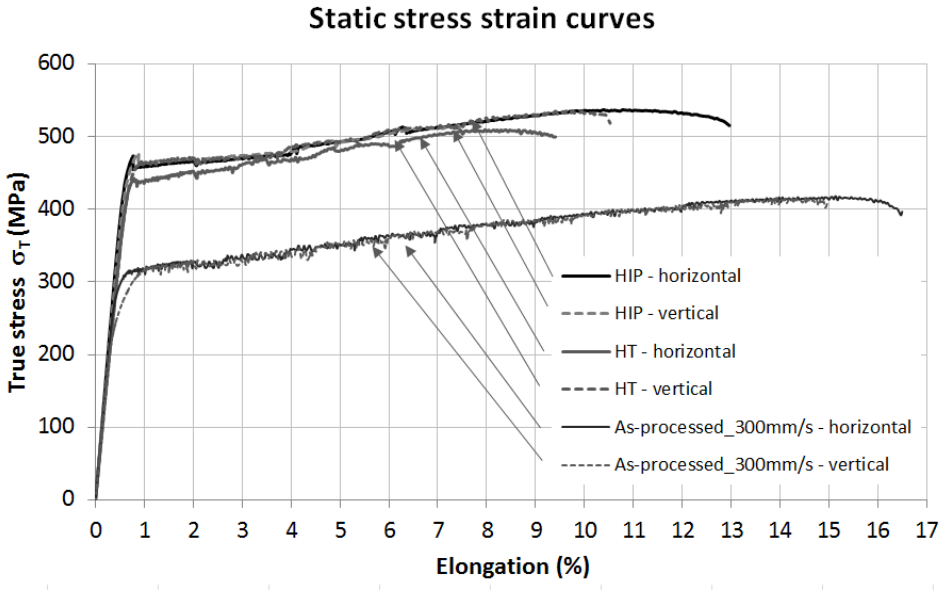

Figure 8: True stress strain curves for as-processed, heat treated and HIPed condition in horizontal and vertical build orientation (DIN 50'125-samples).

However, as expected technical values such as e.g. $R_{m,T}$ and A_5 are slightly different with statistical significance (Figure 6, Table 3), whereas $R_{P0.2}$ values show no statistically significant differences. In all conditions a similar level of strain hardening is obvious. In addition, the Portevin-Le-Chatelier (PLC-) effect takes place, which is typical for Al-Mg alloys as pointed out by Mogucheva et al. [22].

Figure 9 shows fracture surfaces of small cracks in the sample surface of horizontally and vertically built and heat treated samples. It is believed that the origin of such cracks are surface-near pores and connectivity-defects, which had been opened to some extent by the external load, but did not lead to the final fracture. In both build orientations the fracture surfaces show very small dimples, indicating the comparably fine grained, ductile material behaviour. These surface cracks have a length of ≈200µm to 400µm, and lead to significant stress concentrations, as they are displaying very sharp edges.

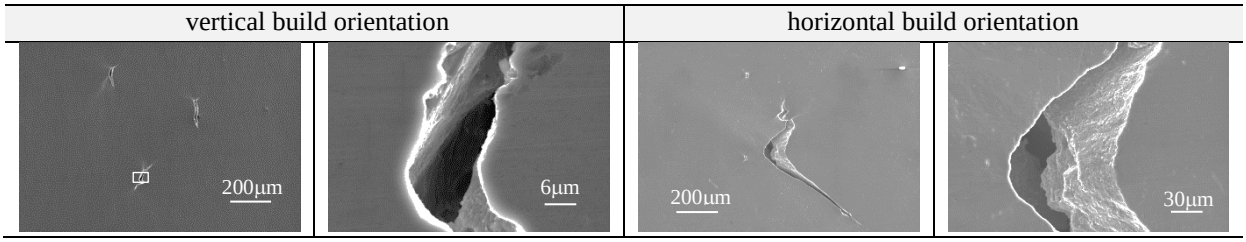

Figure 9: **SEM images of fracture surfaces of horizontal and vertical heat treated samples**

The HIP-ed material properties are shown in Table 3. Obviously, there is a higher anisotropy especially in $R_{m,T}$ compared to the heat treated or as-processed condition. Also the elongation to fracture shows a significant variation.

Table 3: Overview on HIPed material properties for Scalmalloy®

Value	Unit	vertical	horizontal
$R_{m,T}$	MPa	523 ± 18.6	547 ± 4.6
$R_{P0.2}$	MPa	482 ± 4.1	493 ± 13.0
E-Modulus	GPa	76.2 ± 1.7	74.9 ± 1.2
A_5	%	7.7 ± 1.9	10.3 ± 1.4

Differences are significant for $R_{m,T}$ and E, but not for $R_{P0.2}$ (p=0.05)

The fracture surfaces of the HIPed horizontal and vertical samples are shown in Table 4. These surfaces also show some inclusions, but much less internal and surface-near porosity compared to the images shown in Table 4. The fracture orientation is less clearly oriented in a 45° angel to the load axis, as the material is less ductile compared to the as-built condition. However, within the fracture surfaces smaller fracture areas are still displaying an angle in the range of ≈45° to the load axis.

Table 4: Fracture surfaces of HIPed vertical and horizontal samples

vertical build orientation	horizontal build orientation
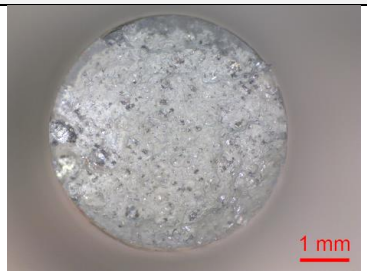	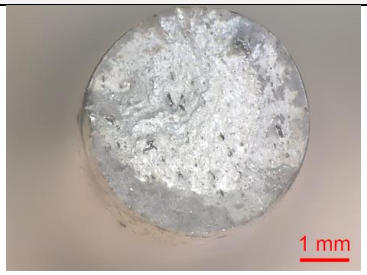
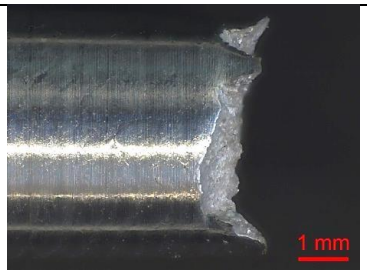	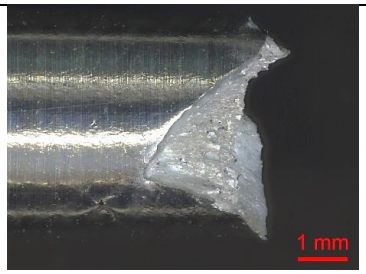

3.4 Microstructure and precipitates in heat treated condition

The microstructure of heat treated (350°C / 4h) material shows basically a very similar bi-modal grain size distribution as in the as-built condition, as shown and discussed in Spierings [12, 14]. Figure 10 shows a BSE-image of the microstructure, where also grain boundary (GB-) particles of higher z-contrast are visible. These particles are identified as oxide particles. The CG-material consists of grains with a size of up to ≈10µm, next to very small partially sub-µm grains. In this context the heat treatment did not change the grain size distribution significantly, as can also be seen from Figure 14.

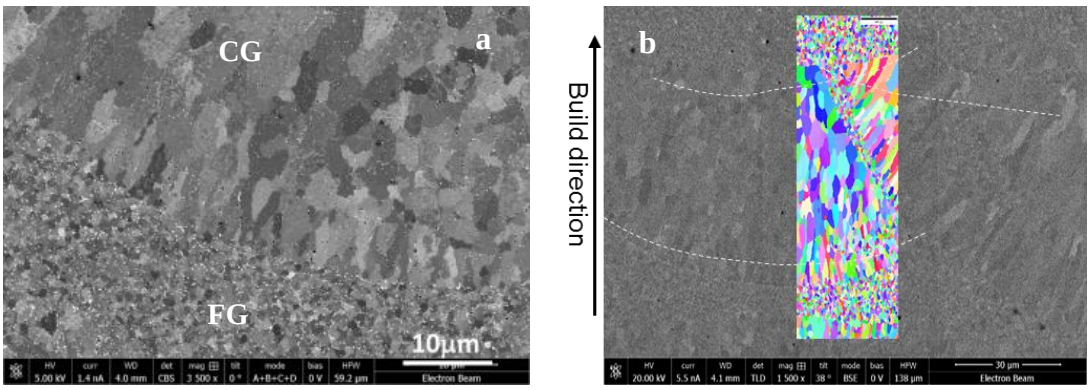

Figure 10: a) Back scattered electron microscopy image of a heat treated (350°C / 4h) sample processed at 170mms^{-1} showing coarse (CG) and fine (FG) grained microstructure, together with high z-contrast particles (white dots). b) EBSD image of a weld-line as discussed in [12]

Figure 11 shows mainly GB-precipitation in fine grained (Figure 11a) and columnar grained (Figure 11b) material. EDS (SEM and STEM) proved that these GB-particles are composed of different oxides, such as SiO_2 with a size of ≈300 nm, identified by z-contrast, but also Fe-Mn rich particles, with traces of Mn, Sc and Zr (Figure 11c).

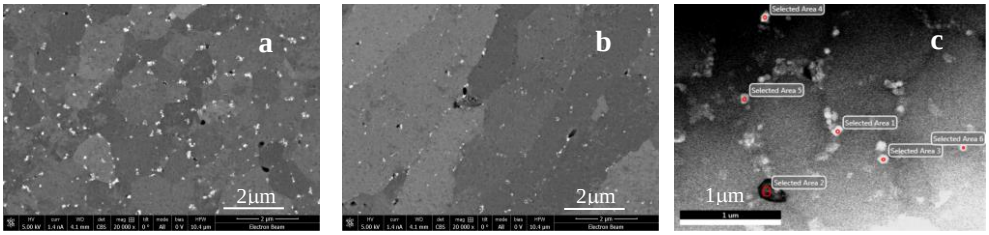

Figure 11: Magnification of Figure 10a: a) FG and b) CG material with GB-oxide particles, and c) HAADF-STEM image showing GB-oxides at higher magnification.

The EDS-analysis in Figure 12 shows the partially complex compositions of the GB-particles. Figure 12a shows an Al-Si-Fe-oxide particle, whereas Figure 12b shows an Al-Mg-oxide with traces of other elements such as Mn, Sc and Zr. The Al-matrix composition was analysed in another scan as 0.6wt% Sc and 4.1wt% Mg, which is close to the nominal composition [12]. Hence, this microstructure is almost identical to the as-built condition.

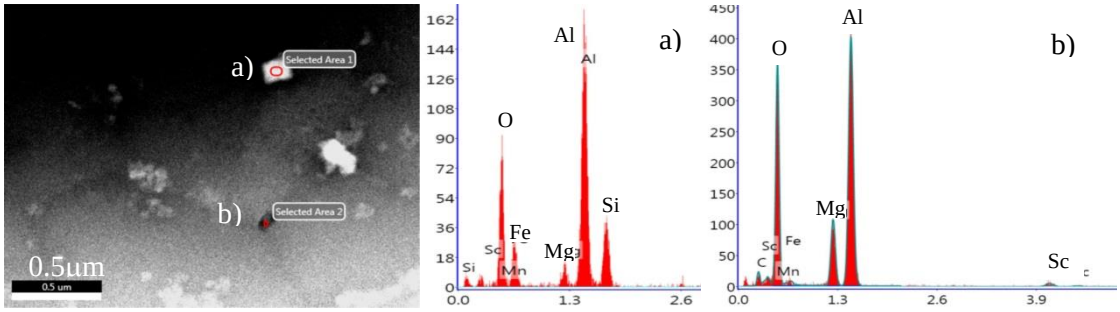

Figure 12: EDS scan in the FG-material of a sample built with 170mms^{-1}. a) shows a complex composition of an oxide with Fe, Mg, Si, and b) is an Al-Mg-oxide with some content of Sc.

3.5 Microstructure and precipitates in HIPed condition

Figure 13 shows the microstructure and corresponding EBSD scan for a HIPed sample produced at v_s = 300mms^{-1}. Obviously, this microstructure looks very similar to the as-built microstructure shown in Spierings [12, 14], with regions of very fine and coarser, partially elongated grains. The [001] pole figures for these two fine grained (FG) and coarser grained (CG) material is very comparable to the as-built condition, with no preferential grain orientation in the FG-region and a preferential grain orientation in the z-direction, hence parallel to the build direction.

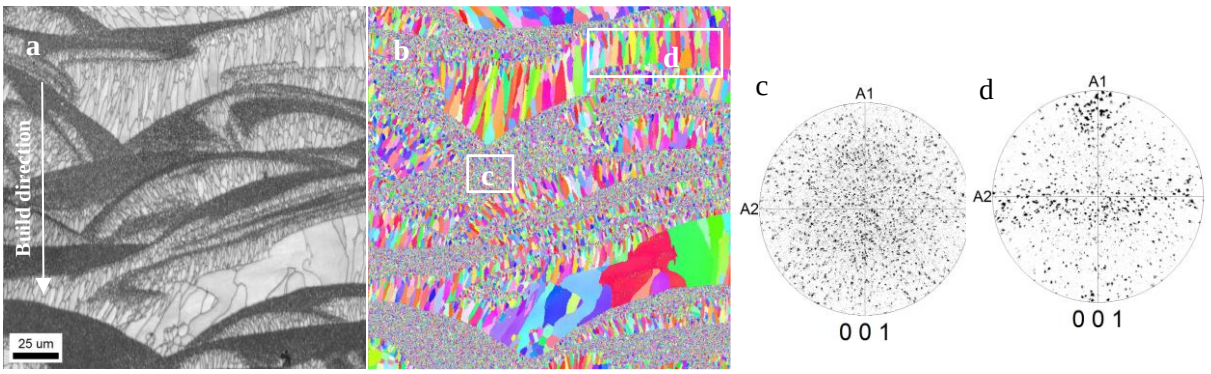

Figure 13: a) Microstructure and b) EBSD of a HIPed sample produced at 300mms^{-1} using the alternate scan strategy shown in Figure 2, showing coarse and fine grained regions. (c) [001] Pole figures for CG (c) and FG region (d).

The grain size distributions in the FG- and CG-region from Figure 13 is shown in Figure 14, together with the distribution in the as-built condition [14]. Obviously the FG-regions are not affected by the heat treatment, with grain sizes <≈ 1.5µm.

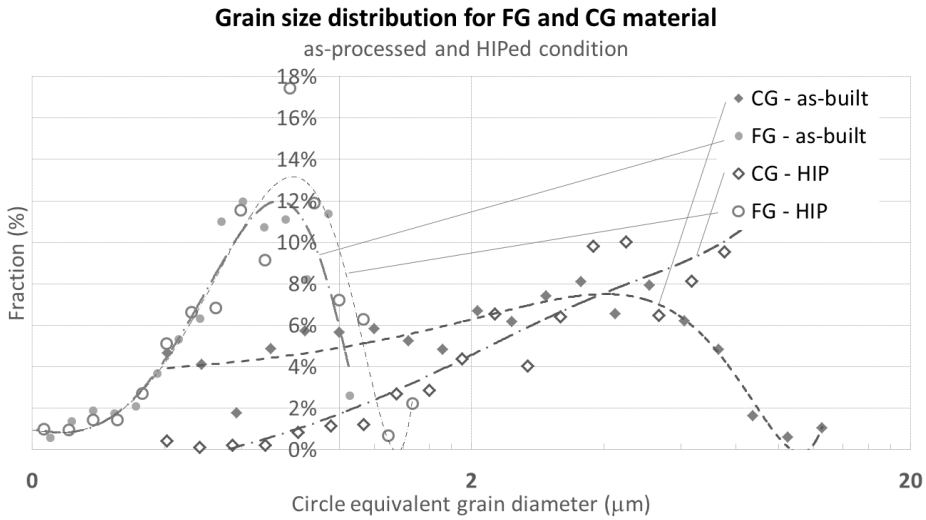

Figure 14: CG- and FG-grain size distribution in as-built and HIPed condition. Grain size in Log-scale.

However, grains in the CG-regions tend to grow on the cost of neighbouring smaller grains, leading to more elongated, larger grains, whereas in the FG-region a significant effect of grain growth cannot be observed. Only in some CG-regions a significant grain growth can be observed, where the grains can reach sizes of up to 20µm to 30µm (dashed line circles in Figure 15a, b), and becoming less columnar as a result of their tendency to reduce surface energy, and the reduction the dislocation density, which were introduced during cool-down of the melt-pool. Next to effects of grain growth, larger Al-oxides, most probably Al_2O_3 inclusions, are formed during HIPing, as visible in Figure 15c.

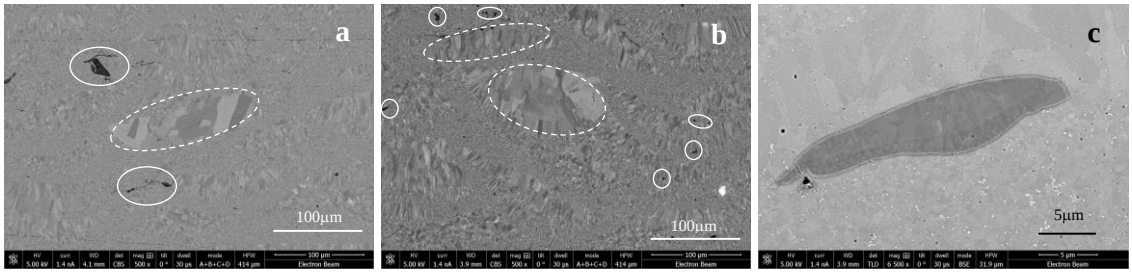

Figure 15: a) Sample manufactured at v_s = 350 mms^{-1} and b, c) at v_s = 550 mms^{-1}, showing grain growth (straight line) and larger Al-oxide inclusions (dashed line). c) Magnification of an Al-oxide particle, with some internal structure

4 Discussion

The ageing development results presented in Figure 3 clearly show that the maximum hardness is achieved at a temperature of 400°C, decreasing rapidly for higher temperatures. This effect can be explained by the potential loss of coherency of nm-scaled $Al_3(Sc_x, Zr_{1-x})$ particles, due to particle growth (Ostwald ripening). Marquis et al. [23] showed in their analysis that at temperatures between 300°C and 400°C the precipitate radii at the higher temperatures are much bigger already at the beginning of a heat treatment, and that they rapidly grow during prolonged ageing times. The limit of ≈400°C for a maximal hardness is also in line with the TTT-diagram developed by Røyset [16], who concluded that at temperatures >370°C discontinuous precipitation starts to take place already at very short holding times of a couple of minutes. The slightly higher temperature limit of 400°C compared to the reported ≈370°C might be explained by the much higher Sc- and Zr- content in this study compared to the alloy used by Røyset and the slower growth rate of $Al_3(Sc_x, Zr_{1-x})$ particles compared to the Zr-free particles [18], together with the associated smaller lattice-misfit of the $Al_3(Sc_x, Zr_{1-x})$ particles.

In contrast, ageing at lower temperatures <≈ 300°C takes a long time for precipitation. Figure 4 shows that at 275°C the hardness reaches the level of a treatment at 325°C / 1h only after prolonged ageing for ≈24h. Therefore, and based on these results the aging temperature should be in the range of 325°C to 350°C. Maximum hardness can then be achieved at hold durations of ≈4h to 5h, with a tendency for even shorter times at 350°C. Figure 4 also shows that such an ageing treatment is very robust with regard to variations in heat treatment temperatures or holding times, and hence the heat treatment oven does not need to fulfil high requirements.

The mechanical properties are very good, and exceed even in the as-built condition (no heat treatment) reported values for other Sc- and Zr- containing alloys. Filatov et al. [24] reported R_m = 360MPa / $R_{P0.2}$ = 280MPa / 20% elongation for a wrought Al-4.2Mg-0.3Sc-0.1Zr alloy, and Fuller [25] measured R_m ≈ 340MPa / $R_{P0.2}$ = 230MPa / ≈11% elongation for a Sc-modified cast 5754 alloy (Al-3.42Mg-0.23Sc-0.22Zr), heat treated at 288°C / 72h. These exceptional mechanical properties of the SLM-processed Scalmalloy® can be associated with the fine-grained microstructure and the (in comparison to the above-mentioned alloys) higher Sc- and Zr- content, which will lead to a higher precipitate volume fraction and therefore more pronounced precipitation hardening. Indeed, heat treated Scalmalloy® reaches tensile strength values >500MPa together with a ductile fracture behaviour. These results on heat treated properties (Figure 6) are basically well in line with values reported by Schmidke [13], especially for $R_{m,T}$. However, the results indicated a slightly lower yield strength $R_{P0.2}$. One possible explanation might be differences in the SLM-machine setup, e.g. filter and smoke evacuation system, which can lead to differences in the remaining porosity level, which in turn directly influences $R_{P0.2}$. This explanation is supported by the results on the HIPed material properties, which are in very good agreement with the findings presented by Palm [26], who used the identical HIP procedure. Another outstanding property of Scalmalloy® is the very low anisotropic mechanical behaviour, which remains <5% for all of the relevant ultimate properties in the as-built, heat treated and HIPed condition. Moreover, there are hardly any differences in the stress-strain behaviour between the two build orientations, and for all material conditions. For other alloys processed by SLM the anisotropy in mechanical property values can reach up to ≈10% and stress-strain behaviour often differs between the build orientations. This positive effect is due to the significantly finer grained microstructure (Figure 14, [14]) compared to other 4xxx alloys, and further supported by the low Hall-Petch constant of aluminium.

The serrations observed in the plastic region of the stress-strain curves are related to the Portevin-Le-Chatelier (PLC) effect, and are typical for Al-Mg alloys, and have been described frequently i.e. by Robinson and Shaw [27] for an Al-4.5wt% Mg alloy, or by Mogucheva [22] for a similar but Sc-modified alloy (Al-4.6Mg-0.35Mn-0.2Sc-0.09Zr). These serrations are typically related to interactions between solute atoms and dislocations. Although the details of these interactions are still under discussion, it seems clear that solute (Mg-) atoms diffuse along the dislocations due to locally stretched atomic lattices,

forming so-called Cottrell clouds. Hence, the dislocations are hindered in their motion and to tear them off a slightly higher stress is required. Once they are released a rapid stress-drop takes place until the dislocations are blocked again, thereby forming the observed serrations (Figure 8). Details about these mechanisms are discussed e.g. by Aboulfadl [28], Robinson [27] and Halim [29]. The PLC effect is classified into three signatures, as discussed by Mogucheva et al. [22]. According to Figure 8 the serrations in the as-processed condition can be identified as type B serrations, which are characterized by stress variations about the general stress-level of the stress-strain curve. In contrast, serrations in the heat treated /HIPed condition are better identified as type A serrations, which are distinguished as rises in the flow stress followed by a drop to or even below the general stress level. Although it is commonly agreed that in Al-Mg alloys especially the Mg-atoms are responsible for dislocation blocking, fine coherent precipitates ($Al_3(Sc_x,Zr_{1-x})$) as they are formed during SLM-processing or by the subsequent heat treatment, also affect the PLC behaviour. Such precipitates and potentially also other particles (Figure 11, Figure 12) are potential obstacles for dislocation movement, and also contribute to the PLC effect, as has been discussed by Zhemchuzhnikova et al. [30] for a similar Al-Mg alloy containing Sc and Zr. This is therefore expected to explain the different PLC-types observed in Figure 8, where in the heat treated condition a higher volume fraction of fine nm-scaled precipitates can be expected. These additional particles together with the Mg-atoms lead to the more hopping type A serrations.

Hence, this PLC-effect also explains the sequence of plastic deformation in a tensile sample, starting locally by the formation of the Lüders Bands, and then spreads continuously over the sample axis. This can be seen in sequence in Figure 7 starting with image b.

The microstructure in the as-built condition is discussed in detail in Spierings et al. [12], showing basically the same bi-modal microstructure as in the heat treated and HIPed condition (Figure 10, Figure 13, Figure 14). No significant changes are found with regard to the fraction of FG- to CG- material, and as in the as-built condition the FG-material does not show any preferential grain orientation (Figure 13c). Similar to the as-built condition, a high number of grain boundary particles of various compositions (partially Sc-enriched Al-Mg-oxides, Fe-Mg-Si oxides) are observed. Such GB-pinning particles are expected to be responsible for the high resistance of the alloy against grain growth, and the good ambient temperature strength properties, as also reported by Fuller [17]. However, HIPing partially tends to lead to grain growth due to the higher energy available from the applied pressure (≥ 1000bar). This grain growth takes place mostly in the CG-regions and preferably in areas where the density of GB-particles is reduced. Such a reduction is related to the specific processing conditions given in SLM, as discussed in Spierings [12]. Hence, areas of larger grains with a more elongated shape (Figure 15a, b) are responsible for the slightly higher anisotropy of the HIPed material ($R_{m,T} \approx 7.5\%$ / $R_{P0.2} \approx 3.7\%$). Correspondingly, also the elongation to fracture is reduced due to a less ductile material behaviour (Table 3). Another effect of HIPing is the formation of larger oxide particles (Figure 15c) with a size up to ≈10 µm. These larger Al-oxides will – due to their different mechanical properties – lead to stress concentrations unter loading, and hence will counterct the positive effect of the pore-free material.

5 Conclusions

Additively processed Sc- and Zr- modified 5xxx alloys such as Scalmalloy® enable the further improvement of mechanical properties by an appropriate heat treatment, favouring the precipitation of fine dispersed $Al_3(Sc_x, Zr_{1-x})$ precipitates.

The following main results are found

- In the as-processed condition a slight dependency of the mechanical properties from the SLM-processing conditions (energy input E_V or scan speed v_s, respectively) is found.
- A post-process heat treatment should be between 325°C and not exceed 350°C, with an aging duration between ≈4h to max. ≈10h to achieve maximal material strength with R_m > 520MPa and $R_{P0.2}$ > 480 MPa.

- Very good mechanical properties are reached in the heat treated condition: $R_{m,T}$ >≈ 500MPa, $R_{P0.2}$ >≈ 450MPa and elongation to fracture > 8.6 ± 1.9%. The associated anisotropy in ultimate values (R_m, A_5) remains < 5%, whereas almost no anisotropy was found in $R_{P0.2}$, which is of significant technical interest. Correspondingly no significant anisotropy was found in the stress-strain behaviour between horizontal and vertical build orientation at a given condition.
- The stress-strain curves show the typical Portevin-Le-Chatelier effect of 5xxx alloys. However, depending on the heat treatment condition different serration types are observed most probably due to different levels of precipitates.
- The evolving bi-modal microstructure is very fine-grained with grain sizes between ≈ 200nm to < 15µm, being even in the coarser regions significantly finer than it is observed in traditionally processed (e.g. cast) aluminium alloys.
- The microstructure in the heat treated condition is not affected, and remains similar to the as-built condition due to the existence of many GB-particles of various compositions preventing grain growth. For this reason Scalmalloy® can sustain high temperatures of up to ≈300°C without losing its properties at room temperature.
- HIPing at 325°C / 4h / 1000bar is suitable to fully eliminate internal pores, and improves the static mechanical properties slightly above the heat treated ones. Especially $R_{P0.2}$ is improved to values above 480MPa. However, due to the higher energy available during the HIP procedure, grain growth in coarse grained areas can take place, leading to a slightly higher anisotropic mechanical behaviour.

These properties make Scalmalloy® an interesting alloy system for various industrial applications, enabling extreme lightweight applications. Further research is required to better understand a potential dependency of the as-built material properties form the SLM-processing conditions.

However, due to the characteristic microstructure formation mechanisms and related good mechanical properties with low anisotropy, this alloying system proves that alloy design for additive manufacturing, taking into account the specific processing conditions given in SLM, enables to significantly improve the resulting material quality. Therefore, alloy design for AM has to be considered as an important aspect in a comprehensive quality management system for AM.

6 Acknowledgements

The authors gratefully acknowledge Mr. M. Demont and Mr. M. Voegtlin for their support in the production of samples and mechanical material analysis. Part of this work has been co-financed by the Swiss Commission for Technology and Innovation, CTI, No. 17365.1.

Literature

[1] E.O. Olakanmi, R.F. Cochranea, K.W. Dalgarno, in: D.L. Bourell (Ed.) Proceedings of the Annual International Solid Freeform Fabrication Symposium, Austin, Texas, 2007.
[2] S. Siddique, M. Imran, E. Wycisk, C. Emmelmann, F. Walther, J. Mater. Process. Technol., 221 (2015) 205-213.
[3] K.G. Prashanth, S. Scudino, H.J. Klauss, K.B. Surreddi, L. Löber, Z. Wang, A.K. Chaubey, U. Kühn, J. Eckert, Mater. Sci. and Eng.: A, 590 (2014) 153-160.
[4] D. Buchbinder, W. Meiners, K. Wissenbach, R. Propawe, in: Fraunhofer Direct Digital Manufacturing Conference 2014, Demmer, A., Berlin, Germany, 2014, pp. 6.
[5] E. Brandl, U. Heckenberger, V. Holzinger, D. Buchbinder, Materials & Design, 34 (2012) 159-169.
[6] D. Manfredi, F. Calignano, M. Krishnan, R. Canali, E.P. Ambrosio, E. Atzeni, Materials, 6 (2013) 856-869.
[7] L. Thijs, K. Kempen, J.-P. Kruth, J. Van Humbeeck, Acta Materialia, 61 (2013) 1809-1819.
[8] T. Kimura, T. Nakamoto, Materials & Design, 89 (2016) 1294-1301.
[9] E.O. Olakanmi, R.F. Cochrane, K.W. Dalgarno, Prog. Mater. Sci., 74 (2015) 401-477.
[10] M. Tang, P.C. Pistorius, JOM, 69 (2017) 516-522.
[11] M.L. Montero Sistiaga, R. Mertens, B. Vrancken, X. Wang, B. Van Hooreweder, J.-P. Kruth, J. Van Humbeeck, Journal of Materials Processing Technology, 238 (2016) 437-445.
[12] A.B. Spierings, K. Dawson, T. Heeling, P.J. Uggowitzer, R. Schäublin, F. Palm, K. Wegener, Materials & Design, 115 (2017) 52-63.
[13] K. Schmidtke, F. Palm, A. Hawkins, C. Emmelmann, Phys. Procedia, 12 (2011) 369-374.
[14] A.B. Spierings, K. Dawson, M. Voegtlin, F. Palm, P.J. Uggowitzer, CIRP Ann. Manuf. Technol., 65 (2016) 213-216.
[15] D. Buchbinder, W. Meiners, N. Pirch, K. Wissenbach, J. Schrage, Journal of Laser Applications, 26 (2014).
[16] J. Røyset, N. Ryum, Mater. Sci. Eng. A, 396 (2005) 409-422.
[17] C.B. Fuller, D.N. Seidman, D.C. Dunand, Acta Materialia, 51 (2003) 4803-4814.
[18] V.G. Davydov, V.I. Elagin, V.V. Zakharov, D. Rostoval, Metal Science and Heat Treatment, 38 (1996) 347-352.
[19] W.F. Hosford, Mechanical Behavior of Materials, Cambridge University Press, New York, 2005.
[20] Y.V. Milman, D.V. Lotsko, O.I. Sirko, Materials Science Forum, 331-337 (2000) 1107-1112.
[21] J. Røyset, N. Ryum, Int. Mater. Rev., 50 (2005) 19-44.
[22] A. Mogucheva, D. Yuzbekova, R. Kaibyshev, T. Lebedkina, M. Lebyodkin, Metallurgical and Materials Transactions A, 47A (2016) 2093-2106.
[23] E.A. Marquis, D.N. Seidman, Acta Mater., 53 (2005) 4259-4268.
[24] Y.A. Filatov, V.I. Yelagin, V.V. Zakharov, Materials Science and Engineering: A, 280 (2000) 97-101.
[25] C.B. Fuller, A.R. Krause, D.C. Dunand, D.N. Seidman, Mater. Sci. and Eng.: A, 338 (2002) 8-16.
[26] F. Palm, K. Schmidtke, in: Proceedings of the 9th International Conference Trends in Welding Research, Chicago 2012.
[27] J.M. Robinson, M.P. Shaw, Materials Science and Engineering, A174 (1994) 1-7.
[28] H. Aboulfadl, J. Deges, P. Choi, D. Raabe, Acta Mater., 86 (2015) 34-42.
[29] H. Halim, D.S. Wilkerson, M. Niewczas, Acta Mater., 55 (2007) 4151-4160.
[30] D.A. Zhemchuzhnikova, M.A. Lebyodkin, T.A. Lebedkina, R.O. Kaibyshev, Materials Science & Engineering A, 639 (2015) 37-41.